TÜBİTAK

Turkish Journal of Earth Sciences

http://journals.tubitak.gov.tr/earth/

Research Article

Turkish J Earth Sci
(2013) 22: 563-573

doi:10.3906/yer-1208-1

Colour origin of red sandstone beds within the Hüdai Formation (Early Cambrian), Aydıncık (Mersin), southern Turkey

Muhsin EREN[1,*] **Selahattin KADİR**[2]

[1]Department of Geological Engineering, Faculty of Engineering, Mersin University, Mersin, Turkey
[2]Department of Geological Engineering, Faculty of Engineering, Eskişehir Osmangazi University, Eskişehir, Turkey

Received: 06.08.2012 • **Accepted:** 28.02.2013 • **Published Online:** 13.06.2013 • **Printed:** 12.07.2013

Abstract: The basal part of the Hüdai Formation (Early Cambrian) in the Aydıncık (Mersin) area comprises red sandstone beds at different stratigraphic levels, showing ripple cross-lamination. These beds were deposited in the middle to lower part of an intertidal flat environment. Bedding-parallel reddening and its cyclic character suggest syn-sedimentary or early diagenetic red colouration in a marine environment. Both X-ray diffraction and petrographic analyses indicate that the red sandstones are composed of predominantly K-feldspar and quartz grains and an illite matrix. These are dominantly arkosic wacke. A small amount of hematite (<5 wt.%) is present in all the samples, which gives a red colour to the whole rock. Scanning electron microscopy images show that hematite pigment appears as spherical and rod-shaped particles in sizes of 1 μm or less disseminated on the grains and in the matrix. Considering their size and morphology, the hematite particles can be interpreted as fossil bacteria, indicating a bacterially induced precipitation, probably from seawater. A 2-step biomineralisation process could explain iron oxidation during early diagenesis in an intertidal environment: (a) trapping of iron (Fe^{2+}) on the bacterial cell wall with oxidation by bacterial activity; (b) inorganic precipitation followed early-stage bacterial nucleation sites resulting in crystal growth. The Fe^{2+} for reddening is provided by an intrastratal alteration of the iron-bearing minerals.

Key words: Arkosic wacke, colour origin, early diagenesis, biomineralisation, Early Cambrian, Hüdai Formation, intertidal red bed

1. Introduction

The term "red beds" usually refers to strata of reddish-coloured sedimentary rocks, which are commonly sandstone, shale, and limestone. They are formed in various depositional environments, including marine and nonmarine environments, and are common in all parts of the stratigraphic record (Van Houten, 1973). The red colour is due to the presence of finely dispersed hematite pigment (Fe_2O_3). The origin of the hematite pigment in red beds is controversial and has been discussed in many papers (Van Houten, 1968, 1973; Einsele, 1992). There are mainly 2 contrasting hypotheses to explain the origin of hematite pigment (Franke and Paul, 1980; Turner, 1980; Pye, 1983; Einsele, 1992; Friedman et al., 1992). One hypothesis contends that the hematite is detritally derived from lateritic soils (e.g., Krynine, 1949; Folk, 1976), and the other hypothesis suggests that the hematite forms authigenetically after deposition by the alteration of iron-bearing detrital grains (e.g., Walker, 1967; Eren and Kadir, 1999). More recently, in the second hypothesis, a microbial origin was proposed for the hematite pigment in carbonate rocks (see Mamet et al., 1997; Preat et al., 1999, 2000; Boulvain et al., 2001; Della Porta et al., 2003; Mamet and Preat, 2006). However, there is no available information regarding a microbial origin of hematite pigment in clastic sedimentary rocks. Most of the knowledge on this subject comes from synthesised microbial (especially bacterial) iron oxidation (e.g., Ehrenreich and Widdel, 1994; Konhauser, 1998; Kapler et al., 2005; Benzerara et al., 2008; Fredrickson and Zachara, 2008; Miot et al., 2009).

This paper investigates the origin of hematite pigment in the red sandstone beds of the Hüdai Formation (Early Cambrian) and provides for the first time evidence for a microbial origin of the red colour in clastic sedimentary rocks.

2. Geological setting

The study area is located within the Aydıncık (Mersin) district, which is known as a part of the central Taurides in southern Turkey (Figure 1; Eren et al., 2007). In the Aydıncık area, a thick sedimentary package ranging in age from the Infra-Cambrian to Recent is present (Figure 2; Koç, 1996; Koç et al., 1997; Eren et al., 2002, 2007). The lower part of this sequence consists of Palaeozoic

* Correspondence: m_eren@yahoo.com

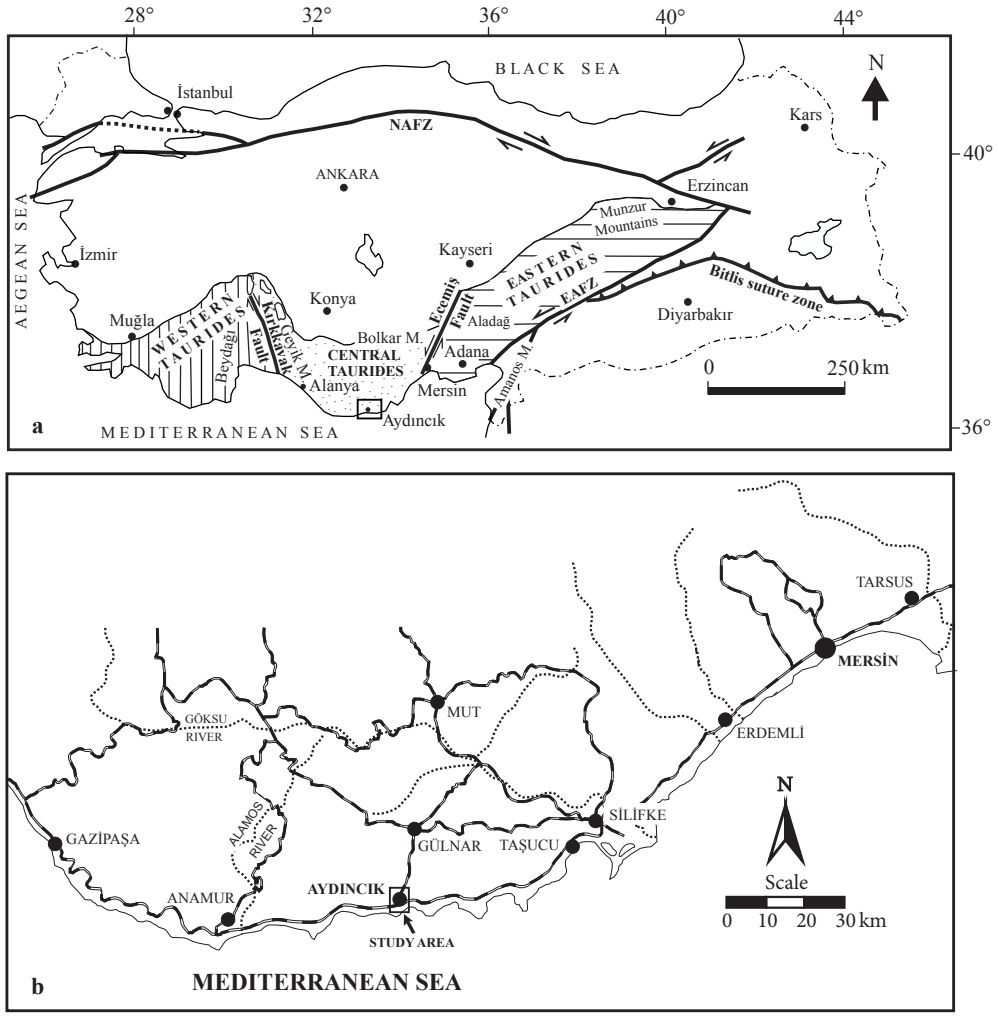

Figure 1. a) Schematic map illustrating the Tauride Orogenic Belt in Turkey and its subdivisions (Eren et al., 2007), NAFZ = North Anatolian Fault Zone, EAFZ = East Anatolian Fault Zone. Study area marked with a square. b) Detailed location map of the study area.

sedimentary/metasedimentary (low-grade metamorphic) units that were deposited at the northern margin of north-eastern Gondwana, describing a preopening period of the Neotethys Ocean (Özgül, 1983; Wehrmann et al., 2010). The Hüdai Formation (Early Cambrian) and its equivalent sedimentary rocks of predominantly cross-bedded quartz-arenites (the Feke Formation) represent the basal part of the Palaeozoic units in the Tauride Belt and are interpreted as beach deposits (Dean and Özgül, 1994; Göncüoğlu, 1995; Kozlu and Göncüoğlu, 1995; Göncüoğlu and Kozlu, 2000). Details of the sedimentary and stratigraphic characteristics of the Hüdai Formation in the Aydıncık area have been provided by Eren and Öner (2000). In the study area, sedimentary rocks of the Hüdai Formation are typically exposed in a cliff near the shoreline and also at Çıra Tepe (hill), where the Hüdai Formation conformably overlies the Sipahili Formation (Infra-Cambrian) at the coastal area and is conformably overlain by the Çaltepe Formation (Lower to Middle Cambrian) (Figure 2; Koç, 1996; Koç et al., 1997; Eren and Öner, 2000). The thickness of the formation is approximately 830 m (Figure 3). In the vertical sequence, the formation represents 3 different parts. The basal part of the formation consists of a rhythmic alternation of a cream-beige, horizontally laminated sandstone (predominantly quartz-arenite), a ripple cross-laminated sandstone (predominantly arkosic wacke), and a green mixed sandstone-shale with shales (Figures 3 and 4a). The middle part is dominated by metashales. The upper part is mainly made up of alternating massive, cream-beige, horizontally laminated sandstones (quartz-arenites) and dark green mixed sandstone-shale, with rare shales of several metres in thickness. In the basal part of the formation, the ripple cross-laminated sandstones often show red colouration. On the bedding surface of

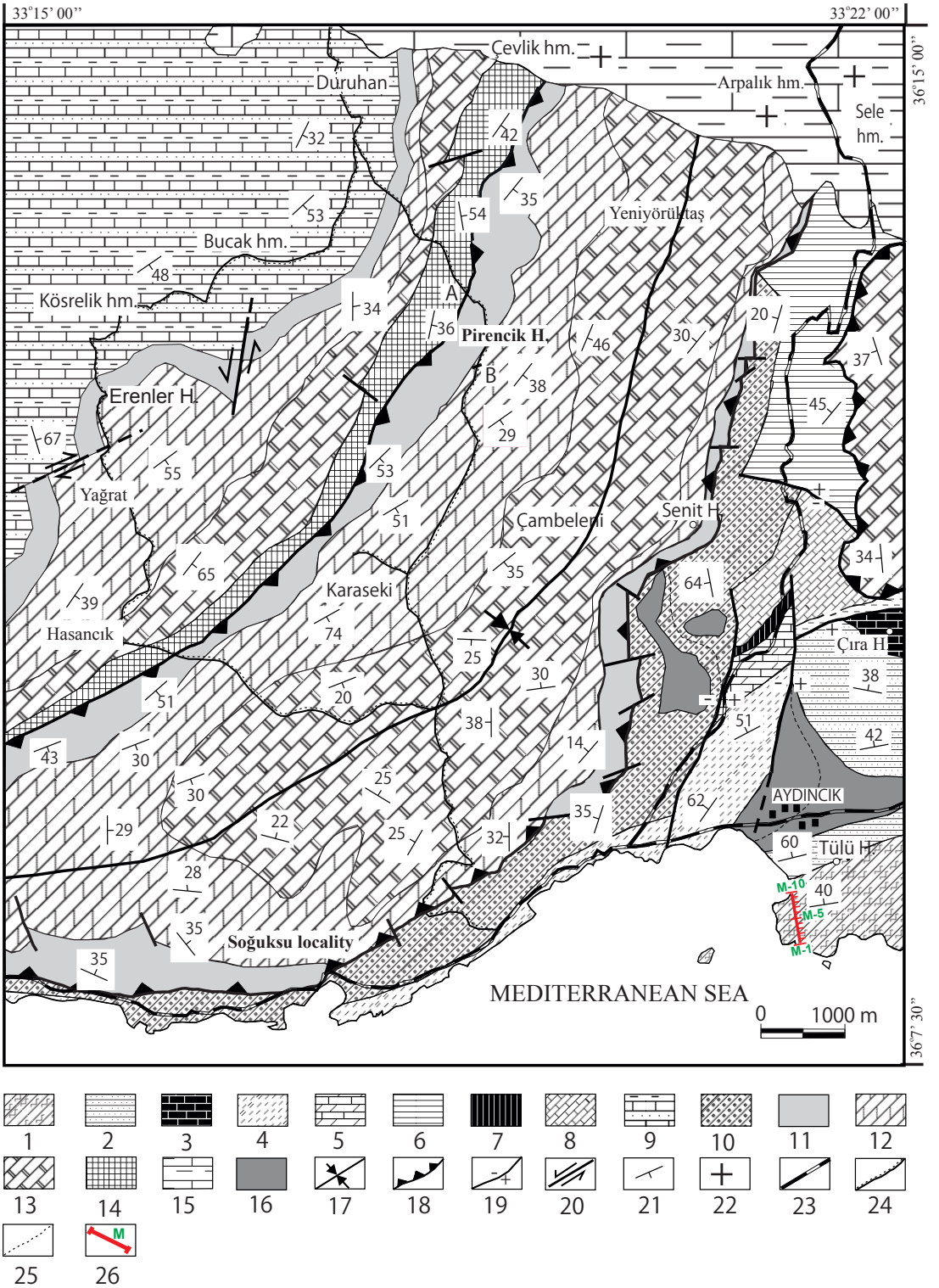

Figure 2. Geological map of the study area (modified from Koç, 1996; Koç et al., 1997). 1- Sipahili Formation (Infra-Cambrian); 2- Hüdai Formation (Early Cambrian); 3- Çaltepe Formation (Early to Middle Cambrian); 4- Seydişehir Formation (Late Cambrian to Ordovician); 5- Büyükeceli Formation (Middle Devonian); 6- Akdere Formation (Late Devonian); 7- Korucuk Formation (Early Carboniferous); 8- Kırtıldağı Formation (Late Permian); 9- Late Palaeozoic (undifferentiated units); 10- Murtçukuru Formation (Late Triassic); 11 to 13- Cehennemdere Formation: 11- Dibekli member (Liassic to Dogger?); 12- Örendüzü member (Dogger to Early Cretaceous?); 13- Çambeleni member (Early Cretaceous); 14- Yavca Formation (Late Cretaceous); 15- Mut Formation (Middle Miocene); 16- alluvium and alluvial terrace (Quaternary); 17- synclinal axis; 18- thrust fault; 19- normal fault; 20- strike slip fault; 21- strike and dip of bedding; 22- horizontal bed; 23- main road; 24- stabilised road; 25- stream; 26- measured section line (M samples).

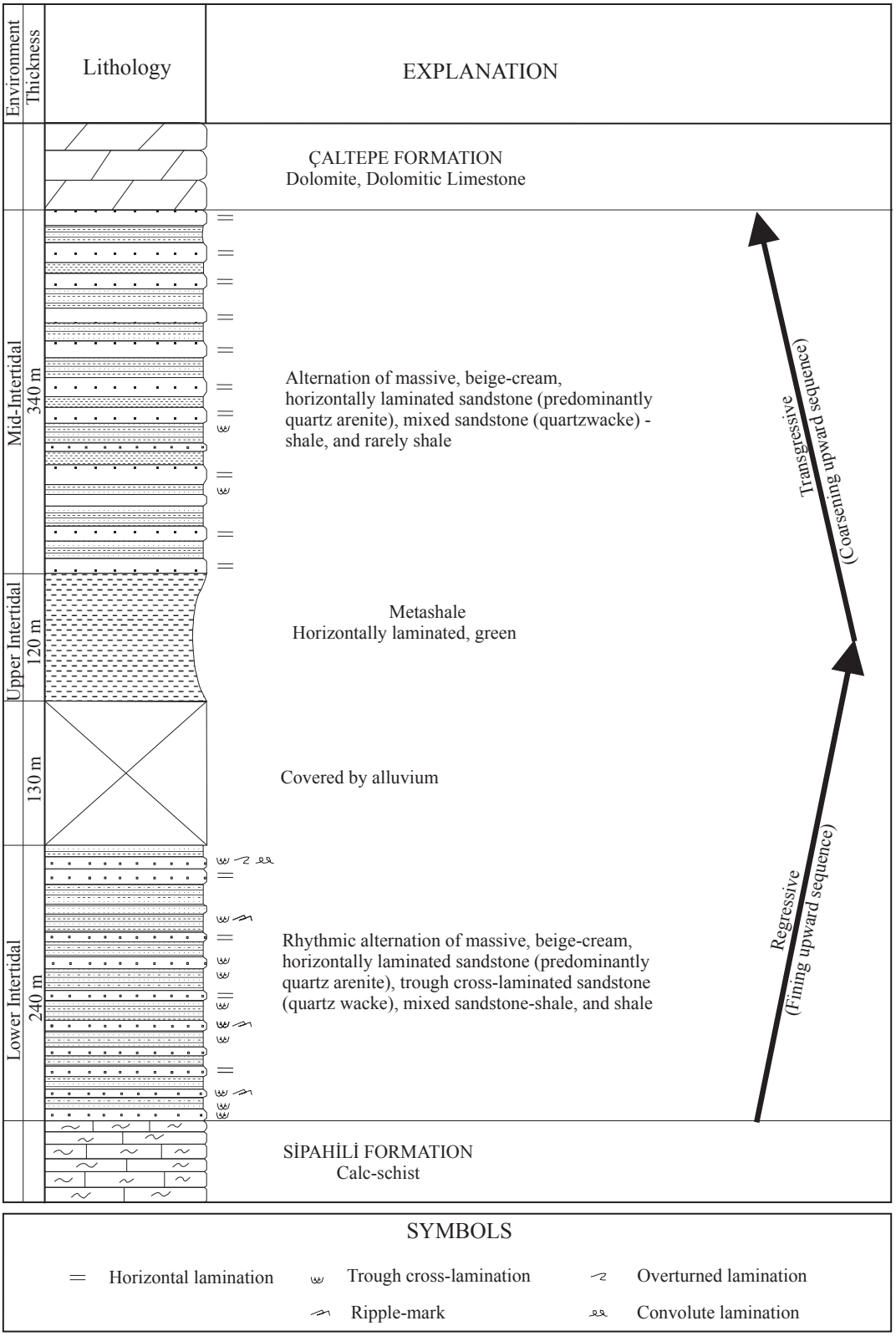

Figure 3. A measured section of the Hüdai Formation showing red beds at the basal part (adapted from Eren and Öner, 2000).

the red beds, various ripple types are present, including symmetrical, asymmetrical, and interference patterns (Figure 4). The sedimentary characteristics of the red beds suggest deposition in tidal flat environments (Klein, 1970; Boggs, 1987; Tucker, 1991; Eren and Öner, 2000). Petrographic examination and X-ray diffraction (XRD) analysis (Figure 5) reveal that the grains in the sandstones of the Hüdai Formation are predominantly monocrystalline quartz and K-feldspar (orthoclase) with negligible or trace amounts of microcline, plagioclase (oligoclase), mica, pyroxene, zircon, tourmaline, and apatite (Eren and Öner, 2000). Rock fragments are absent in these sediments. These mineralogical components suggest that the source rock for these sediments was a granite or a granite gneiss (Robb, 1949), indicating continental provenances based on the geotectonic classification of Dickinson and Suczek (1979).

3. Materials and methods

During the field work, 10 representative samples of red sandstone beds were collected along a stratigraphic section (lower part; Figures 2, 3, and 4a), which was discussed in a previous paper (Eren and Öner, 2000). The stratigraphic section was measured from the present-day coastline to Çıra Tepe (hill). Thin sections were prepared from the samples and examined via polarised-light microscopy (Leitz Laborlux 11 Pol). Mineralogical and chemical compositions of the selected samples were characterised by XRD (Rigaku-Geigerflex) and X-ray fluorescence (XRF) (Rigaku X-ray spectrometer RIX 3000) analyses at the General Directorate of Mineral Research and Exploration (MTA), Ankara, Turkey. Loss on ignition (LOI) for each sample was also determined by drying the samples at 105 °C overnight, followed by determination of their water (and other volatiles) contents at 1050 °C.

Semiquantitative estimations of mineral abundance in the whole rock were obtained by using intensities of the basal reflections of each mineral in the XRD patterns. Scanning electron microscopy and energy-dispersive analyses (SEM-EDX) (JEOL JSM 84A-EDX) were performed at Middle East Technical University, Ankara, Turkey. Representative red sandstone samples were prepared for SEM-EDX analysis by adhering the fresh, broken surface of each rock sample onto an aluminium sample holder using double-sided tape, and then coated with a thin film (~350 Å) of gold using a Giko ion coater.

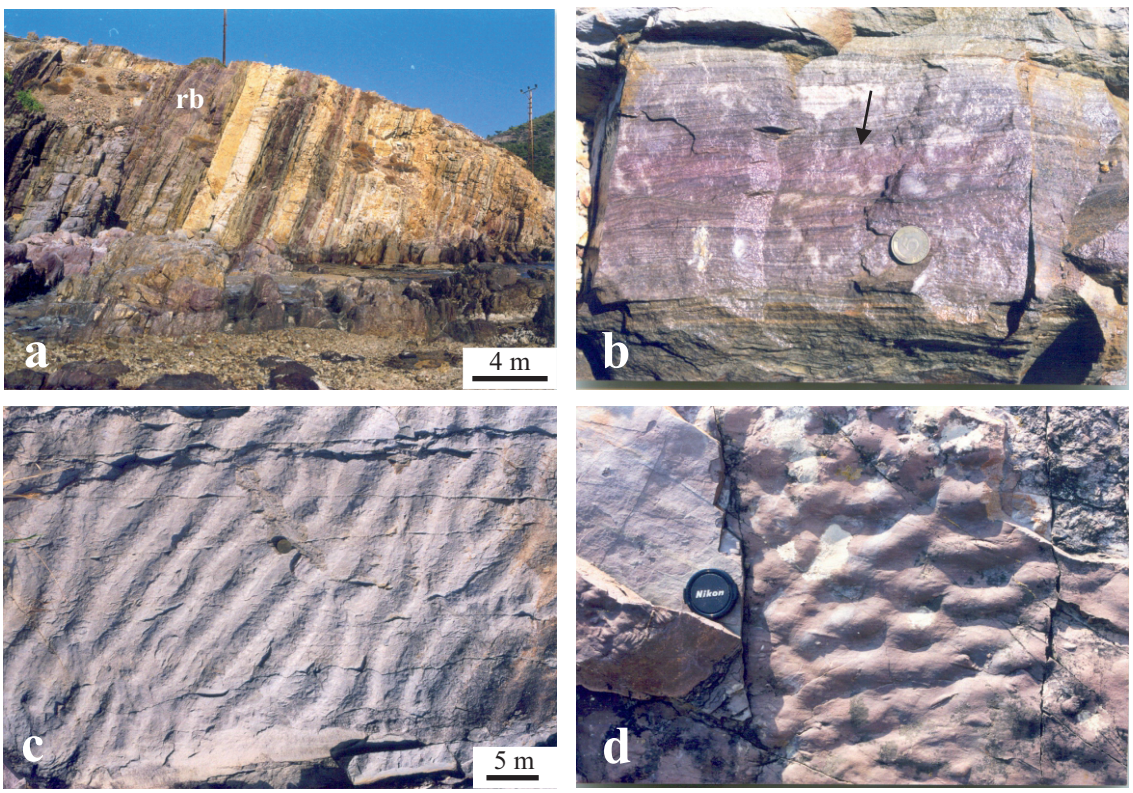

Figure 4. Field photographs of red beds and associated sedimentary structures: a) an excellent exposure of the Hüdai Formation (Early Cambrian) showing red bed intercalations (rb); b) examples of sedimentary structures in outcrops indicating characteristics of intertidal environment, with typical cross-lamination (arrow) in the red sandstones showing a colour change from red to greenish grey along the bedding surface; c) wave ripples on the bedding surface of red beds, d) interference ripples on the bedding surface of red beds.

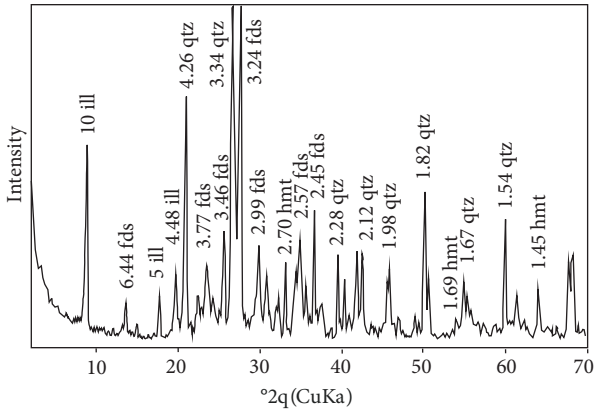

Figure 5. X-ray diffraction pattern of a typical red sandstone sample (arkosic wacke; sample no. M-2), showing reflections of quartz (qtz), K-feldspar (fds), illite (ill), and hematite (hmt). Intensities of reflections are related to abundance of minerals.

4. Results

XRD analysis of the red sandstones revealed a predominance of K-feldspar, quartz, and illite (Table 1; Figure 5). Petrographic investigation reveals that in the red sandstones, K-feldspar and quartz are the dominant detrital constituents, and illite is present as a matrix between grains, indicating a predominantly arkosic wacke (Figure 6a) and a rarely arkosic sandstone (Table 1; Pettijohn et al., 1987). The red sandstones contain SiO_2 and Al_2O_3 values ranging from 68 to 86 wt.% and from 5 to 14 wt.%, respectively. Relatively high SiO_2 and K_2O values are linked to the presence of quartz and K-feldspar grains and the illite matrix.

In thin section, trace amounts of detrital hornblende, muscovite, tourmaline, biotite, opaque minerals, and large hexagonally shaped authigenic hematite crystals (Figure 6b) are also present. In all the samples, hematite was determined to be an accessory mineral. Hematite content ranges from 2% to 6%. The large hematite crystals are interpreted to be of late diagenetic origin because of their cross-cutting relationship with the other minerals (Figure 6c). Whole-rock SEM analyses confirm the presence of feldspar and quartz grains and an illite matrix (Figures 6d–6g).

XRF analyses were carried out on all the samples to determine the chemical composition of the red beds, and the results are given in Table 2. In the samples, Fe_2O_3 values ranged from 1.7 to 5.0 wt.%, whereas FeO values ranged from 0.45 to 0.90 wt.%.

Hematite pigment appears as spherical (cf. Casanova et al., 1999) and rod-shaped (or bacillus-shaped, cf. Benzerara et al., 2008; Miot et al., 2009) particles in sizes of ~1 μm or less disseminated on the detrital grains and illite flakes in the matrix. The EDX analyses of hematite pigment exhibit strong peaks of Fe but poor Si, Al, and K, indicating the presence of accessory illite accompanying the hematite (Figure 6h).

5. Discussion

The red beds in the Hüdai Formation were deposited in the middle and lower part of an intertidal flat environment (Larsonneur, 1975; Eren and Öner, 2000) because of various associated ripples (Figure 4). Similar red beds in a shallow marine environment have been reported by Turner (1979). In the Hüdai Formation, the reddening is restricted by bedding surfaces and repeats in the sequence, representing syn-sedimentary or early diagenetic colouration. The reddening is caused by finely dispersed hematite (Fe_2O_3; Van Houten, 1973; Turner, 1980; Al-Rawi, 1983; Einsele, 1992; Friedman et al., 1992; Eren and Kadir, 1999). The XRF and XRD analyses showed that very small quantities of hematite pigment caused reddening in the sediments (Tables 1 and 2; Figures 6d–6g; see also Walker, 1967; Tucker, 1991). Jimenez-Espinosa and Jimenez-Millan (2003) suggested that the hematite formation would

Table 1. Semiquantitative mineralogical compositions of 10 representative red sandstone samples (by wt.%).

Sample	Quartz	Feldspar	Illite	Hematite
M-1	18	71	9	2
M-2	11	45	41	3
M-3	12	55	30	3
M-4	15	68	13	4
M-5	12	56	26	6
M-6	17	67	14	2
M-7	13	62	20	5
M-8	14	58	25	3
M-9	14	58	23	5
M-10	10	41	45	4

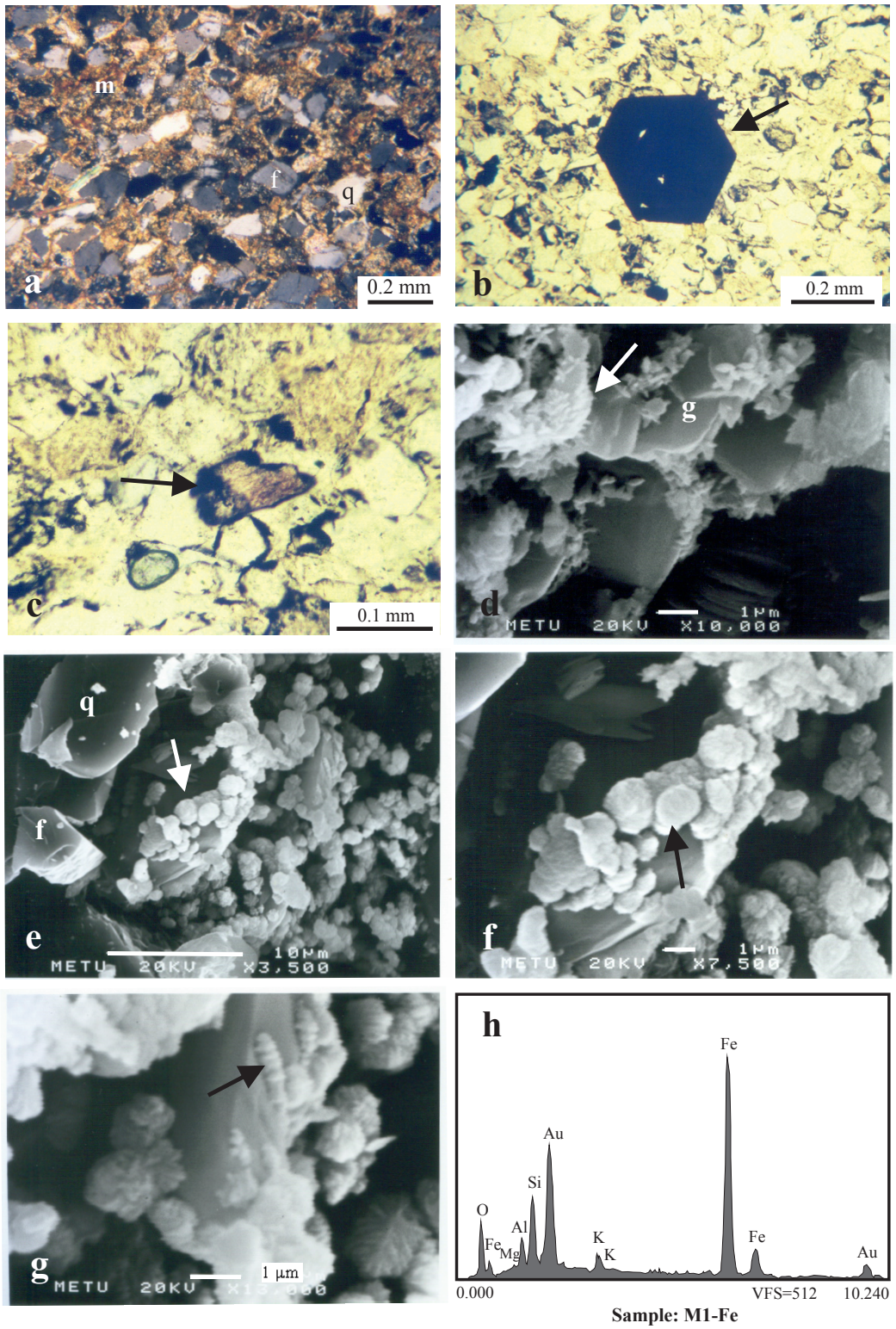

Figure 6. Micrographs of red sandstones and EDX spectra of hematite pigment: a) typical thin-section view of red sandstone (arkosic wacke) in cross-polarised light, q = quartz, f = feldspar, m = clay matrix; b) late diagenetic hematite in a thin section illustrating a euhedral hexagonal crystal form (arrow), in plane-polarised light; c) thin-section view of an iron-oxidised/-hydroxised halo (arrow) around detrital mica grain, in plane-polarised light; d) SEM view of hematite pigment (arrow) showing a patchy coating on detrital grains (g); e) SEM view of spherical hematite particles (arrow), q = quartz, f = feldspar; f) close-up of Figure 6e; g) rod-shaped (or bacillus-shaped) hematite particles (arrow) disseminated on the grain surface; h) EDX spectrum of hematite pigment with adjacent clay matrix (illite).

Table 2. Chemical compositions of 8 red sandstone samples (oxides in wt.%).

Major oxides (wt.%)	M-1	M-2	M-3	M-4	M-6	M-7	M-8	M-10
SiO_2	82.0	74.5	72.6	85.5	80.0	74.0	73.8	68.0
Al_2O_3	8.2	11.0	11.5	5.5	9.0	11.5	12.6	13.5
K_2O	6.6	8.7	9.1	4.1	6.6	8.0	8.7	9.4
FeO	0.5	0.7	0.6	0.65	0.45	0.65	0.55	0.9
tFe_2O_3	1.7	3.0	4.0	3.5	2.1	4.5	3.2	5.0
Na_2O	0.2	0.2	0.3	0.2	0.2	0.2	0.3	0.3
MgO	0.4	0.6	0.7	0.2	0.5	0.5	0.5	1.0
P_2O_5	0.1	0.2	0.2	0.1	0.1	0.1	0.1	0.2
CaO	0.1	0.3	0.3	0.1	0.1	0.1	0.1	0.3
TiO_2	0.1	0.7	0.6	0.2	0.3	0.3	0.5	0.6
MnO	0.1	0.1	0.1	0.1	0.1	0.1	0.1	0.1
LOI	0.15	0.65	0.5	0.1	0.75	0.85	0.75	1.0
Total	99.65	99.95	99.9	99.6	99.75	100.15	100.65	99.4

tFe_2O_3 = total iron oxides, LOI = loss on ignition at 1050 °C.

require enough moisture to enable chemical weathering of iron-bearing primary minerals such as amphibole, biotite, and related iron (oxyhydr)oxides and a low water activity to propel dehydration. Low pH conditions in acidic water are favourable for the dissolution of Fe-bearing silicates to release the ferrous iron (Fe^{2+}). The dissolution rates of these minerals decrease with rising pH and low temperatures, are lowest at near-neutral pH, and rise again when pH is in the alkaline range (Burns, 1993). The acidic pH (about 3–3.5) may have resulted in the precipitation of iron (oxyhydr) oxides such as goethite, lepidocrosite, and hematite (Schwertmann, 1993; Kampf et al., 2000). Ferrous iron (Fe^{2+}) is oxidised to ferric form (Fe^{3+}) at neutral or alkaline pH conditions (Stumm and Morgan, 1996; Mamet et al., 1997). Chemical weathering of primary minerals in the red beds is characterised by an iron (oxyhydr)oxide halo around biotite (Walker, 1967) in the thin sections (Figure 6c), which indicates intrastratal alteration (Walker et al., 1981; Al-Rawi, 1983). Hematite crystallisation requires very high temperatures or environments wherein the water activity is considerably reduced. In the Hüdai Formation, the dissolution and subsequent hematite authigenesis took place principally within the marine phreatic and/or vadose zones where normal marine water is well oxygenated. In the red beds, alteration partially removes hematite pigment, especially along bedding surfaces where the red colour is converted to green. The green colour indicates the original colour of the sediments before reddening, which reflects reducing conditions or presence of ferrous iron in chlorite and illite and the absence of hematite, iron sulphides, and organic matter (McBride, 1974; Myrow, 1990). Reducing conditions in well-oxygenated water may be provided by micropores in matrix-supported sandstones that impede circulation of oxygen and favour colonisation by iron bacteria (Boulvain et al., 2001). Cyclic reddening is related to oxygen fluctuations in the depositional environment, probably resulting from a sea-level change. Reducing conditions are generated below the sediment–water interface where ferrous iron (Fe^{2+}) is dissolved at low temperatures. Lowering of the sea level then causes the sediments to be in more oxidised conditions, under which hematite forms at probably high temperatures.

The spherical and rod-shaped (or bacillus-shaped) morphologies of hematite particles are interpreted as fossil bacteria (Figures 6d–6h), suggesting a bacterially induced precipitation, probably from seawater. Bacteria have long been recognised for their ability to oxidise iron inside and outside of their cell structures, but the mechanism for the microbial iron oxidation is not yet fully understood. Iron is present as Fe^{2+} in primary minerals (mainly silicates) and is released during weathering in an acidic environment at low pH. Microorganisms effectively influence the kinetics of mineral alterations and formation reactions (Ehrlich, 1998; Rogers and Bennett, 2004). They interact strongly with mineral surfaces and enhance weathering through the supply of acid and strong complexing ligands (Churchman, 2000).

Some microorganisms such as bacteria are able to actively oxidise Fe^{2+} in aqueous solutions. These are called iron bacteria (Schwertmann and Taylor, 1989). Iron oxidation is mainly controlled by pH and oxygen (Crichton, 1991). Fortin and Langley (2005) summarised the possible processes involved in the bacterially induced iron oxidation. Biogenic iron oxide forms either as a result of direct metabolic activity or passive sorption and nucleation reaction. The metabolic activity of acidophilic (e.g., *Thiobacillus ferrooxidans*) and neutrophilic (e.g., *Gallionella ferruginea* and *Leptothrix discophora*) iron-

oxidising bacteria under oxic conditions supports the oxidation of Fe^{2+} to Fe^{3+} and the precipitation of biogenic iron oxides as extracellular precipitates near or on the bacterial cell. Iron oxidation under anoxic conditions can also occur as a result of the activity of nitrate-reducers and photoautotrophic bacteria using Fe^{2+} as an electron donor (Fortin and Langley, 2005; Miot et al., 2009). Passive iron sorption and nucleation onto bacterial cell walls represents another mechanism leading to iron oxide formation. The surface reactivity of bacteria under environmental pH conditions gives a net negative charge to the cell wall, which leads to the binding of soluble iron and eventually to the precipitation of iron oxides under saturation conditions. Extracellular polymers produced by bacteria can act as a template for iron sorption and iron oxide nucleation. Another pathway in metabolic oxidation is intracellular iron oxide formation, which can be achieved by a large variety of heterotrophic microorganisms. In the intracellular iron oxide formation, enzymes are biological catalysts that lower the activation energy so that chemical reactions can occur within a living cell (Atlas, 1995). Konhauser (1998) suggested that the vast majority of bacterial biomineralisation occurs in a 2-step process: the metals are initially electrostatically bound to the anionic surfaces of the cell wall and the surrounding organic polymers, where they subsequently serve as nucleation sites for crystal growth. In the first stage, free Fe^{2+} would bind to negatively charged polymers and then be oxidised in a polymer matrix, possibly by iron-oxidising enzymes or iron-oxidising factors excreted by the bacteria (Ghiorse, 1984). The later-stage mineralisation is inorganically driven and characterised by surface irregularities on the bacteria-shaped particles.

Sedimentary characteristics of the red beds in the Hüdai Formation suggest deposition in a tidal flat environment where wave actions and tidal bottom currents were effective. The dynamic processes of the tidal flat environment suggest well-oxygenated water and probably circumneutral pH values. However, the matrix-rich sandstones indicate relative low-energy conditions. The SEM images show that bacteria grew on the grain surfaces and clay particles in the matrix micropores (Figures 6d–6g), whose characteristics were probably different than those of the macroenvironment. The previous green colour of the red beds, as mentioned above, suggests that free oxygen concentration was very low in the micropores and dysaerobic conditions prevailed. Under low-oxygen conditions, inorganic iron oxidation rates are very slow (Santelli et al., 2001). Furthermore, Jørgensen (1982) suggested that the oxygen concentration drops to zero within a few millimetres below the surface of the marine coastal sediments. In anoxic environments, microorganisms can use Fe^{3+} oxyhydroxide phases as electron acceptors for respiration of organic compounds (Ehrlich, 1996), thereby probably increasing the local acidity of the water, catalysing the weathering of iron bearing minerals, and releasing Fe^{2+} into solution. The iron silicate dissolution reactions provide nutrients for microorganisms and therefore these reactions could sustain a significant microbial population (Santelli et al., 2001; Rogers and Bennett, 2004).

Overall, the SEM images suggest that bacterially induced precipitation led to the hematite pigment. However, morphology alone is not sufficient to identify spheroidal and rod-shaped bodies. These morphologies differ from the idea of photosynthetic bacteria forming as encrusting sheaths or mats on the sediment surface and consisting of filamentous species. Therefore, we conclude that the microorganisms involved in the iron oxidation were nonphotosynthetic. The bacteria could initiate or at least positively influence the iron oxide precipitation, which is the result of either direct (metabolic assimilation for the production of energy) or indirect (sorption, microenvironmental changes) factors (Casanova et al., 1999). After the bacterially induced nucleation, inorganic iron oxide mineralisation continued around the nuclei until the system reached equilibrium (Konhauser, 1998). This is characterised by the surface irregularities on the bacteria-shaped particles. The cyclic reddening in the sequence also indicates an effect of the macroenvironmental changes. A lowering sea level or low tide in the intertidal flat environment, indicated by the flat-topped ripple marks, caused more oxygenated conditions in both the macro- and microenvironments and resulted in pervasive oxidation throughout the bed.

6. Conclusion

Red beds are common at the basal part of the Hüdai Formation (Early Cambrian) deposited in an intertidal flat environment. Sedimentary structures with bedding parallel reddening and its cyclic character suggest syn-sedimentary or early diagenetic colourisation resulting from a small amount of disseminated hematite pigment. Spherical and rod-shaped (or bacillus-shaped) morphologies of hematite particles suggest a bacterially induced precipitation, probably from seawater, which later serves as nucleation sites for crystal growth during the sea-level changes in the intertidal environment. However, the reddening is mainly controlled by oxygen fluctuations in the depositional environment resulting from the lowering sea level. Under these conditions, bacteria could initiate, or at least positively influence, the iron oxide precipitation.

Acknowledgements

The authors are indebted to the anonymous reviewers for their careful and constructive reviews, which significantly improved the quality of the paper. They are also grateful to Professor Ömer Işık Ece (editor) for his insightful editorial comments and suggestions.

References

Al-Rawi Y (1983). Origin of red color in the Gercus Formation (Eocene), northeastern Iraq. Sediment Geol 35: 177–192.

Atlas RM (1995). Microorganisms in Our World. St. Louis, Missouri, USA: Mosby.

Benzerara K, Miot J, Morin G, Kapler A, Obst M (2008). Biomineralization by iron-oxidizing bacteria. In: Dalzell M, editor. Canadian Light Source Activity Report 2008. Saskatoon: Canadian Light Source, Inc., pp. 86–87.

Boggs S Jr (1987). Principles of Sedimentology and Stratigraphy. New York: Macmillan.

Boulvain F, De Ridder C, Mamet B, Preat A, Gillan D (2001). Iron microbial communities in Belgian Frasnian carbonate mounds. Facies 44: 47–60.

Casanova J, Bodenan F, Negrel P, Azaroual M (1999). Microbial control on the precipitation of modern ferrihydrite and carbonate deposits from the Cezallier hydrothermal springs (Masif Central, France). Sediment Geol 126: 125–145.

Crichton RR (1991). Inorganic Biochemistry of Iron Metabolism. Chichester, UK: Ellis Horwood.

Churchman GJ (2000). The alteration and formation of soil minerals by weathering. In: Sumner ME, editor. Handbook of Soil Science. Boca Raton, Florida, USA: CRC Press, pp. F3–F76.

Dean WT, Özgül N (1994). Cambrian rocks and faunas, Hüdai area, Taurus Mountains, southwestern Turkey. Bull Inst Roy Sci Nat Belg 64: 5–20.

Della Porta G, Mamet B, Preat A (2003). Microbial mediation in the formation of red limestones, Upper Carboniferous, Cantabrian Mountains, Spain. In: Wong TE, editor. Proceedings of the XVth International Congress on Carboniferous and Permian Stratigraphy, Utrecht, the Netherlands, pp. 243–250.

Dickinson WR, Suczek CA (1979). Plate tectonic and sandstone composition. AAPG Bulletin 63: 2164–2182.

Ehrenreich A, Widdel F (1994). Anaerobic oxidation of ferrous iron by purple bacteria, a new type of phototrophic metabolism. Appl Environ Microbiol 60: 4517–4526.

Ehrlich HL (1996). Geomicrobiology. New York: Marcel Dekker.

Ehrlich HL (1998). Geomicrobiology: its significance for geology. Earth Sci Rev 45: 454–460.

Einsele G (1992). Sedimentary Basins – Evolution, Facies, and Sediment Budget. Berlin: Springer.

Eren M, Kadir S (1999). Colour origin of upper cretaceous pelagic red sediments within the eastern Pontides, northeast Turkey. Int J Earth Sci 88: 593–595.

Eren M, Kaplan MY, Kadir S (2007). Petrography, geochemistry and origin of Lower Liassic dolomites in the Aydıncık area, Mersin, southern Turkey. Turkish J Earth Sci 16: 339–362.

Eren M, Öner F (2000). Sedimentary characteristics of the Hüdai Formation (Early Cambrian) within the Aydıncık (İçel), S Turkey. Ann Soc Geol Pol 70: 251–259.

Eren M, Taslı K, Tol N (2002). Sedimentology of Liassic carbonates (Pirencik Tepe measured section) in the Aydıncık (İçel) area, southern Turkey. J Asian Earth Sci 20: 791–801.

Folk RL (1976). Reddening of desert sandstone: Simpson Desert, N.T., Australia. J Sediment Petrol 46: 604–615.

Fortin D, Langley S (2005). Formation and occurrence of biogenic iron-rich minerals. Earth Sci Rev 72: 1–19.

Franke W, Paul J (1980). Pelagic redbeds in the Devonian of Germany – deposition and diagenesis. Sediment Geol 25: 231–256.

Fredrickson JK, Zachara JM (2008). Electron transfer at the microbe-mineral interface: a grand challenge in biogeochemistry. Geobiology 6: 245–253.

Friedman GM, Sanders JE, Kopaska-Merkel DC (1992). Principles of Sedimentary Deposits: Stratigraphy and Sedimentology. New York: Macmillan.

Ghiorse WC (1984). Biology of iron- and manganese-depositing bacteria. Annu Rev Microbiol 38: 515–550.

Göncüoğlu MC (1995). Distribution of Lower Paleozoic rocks in the Alpine Terranes of Turkey: Paleogeographic constraints. In: Göncüoğlu MC, Derman AS, editors. Early Paleozoic Evolution in NW Gondwana. TAPG Special Publication 3, pp. 13–23.

Göncüoğlu MC, Kozlu H (2000). Early Paleozoic evolution of the NW Gondwanaland: data from Southern Turkey and surrounding regions. Gondwana Res 3: 315–324.

Jimenez-Espinosa R, Jimenez-Millan J (2003). Calcrete development in Mediterranean colluvial carbonate systems from SE Spain. J Arid Environ 53: 479–489.

Jørgensen BB (1982). Mineralization of organic matter in the sea bed – the role of sulphate reduction. Nature 296: 643–645.

Kampf N, Scheinost AC, Schulze DG (2000). Oxide minerals. In: Sumner ME, editor. Handbook of Soil Science. Boca Raton, Florida, USA: CRC Press, pp. 125–168.

Kappler A, Schink B, Newman DK (2005). Fe(III) mineral formation and cell encrustation by the nitrate-dependent Fe(II)-oxidizer strain BoFeN1. Geobiology 3: 235–245.

Klein GD (1970). Tidal origin of a Precambrian Quartzite; the lower fine-grained quartzite (Middle Dalradian) of Islay, Scotland. J Sediment Petrol 40: 973–985.

Koç H (1996). Stratigraphy and Geotectonic Interpretation of Aydıncık (İçel) Area. MS thesis, Mersin University, Mersin, Turkey [unpublished, in Turkish].

Koç H, Özer E, Özsayar T (1997). Geology of Aydıncık (İçel) area. Geosound Earth Sci 30: 417–427.

Konhauser KO (1998). Diversity of bacterial iron mineralization. Earth Sci Rev 43: 91–121.

Kozlu H, Göncüoğlu MC (1995). Stratigraphy of the Infra-Cambrian rock-units in eastern Taurides and their correlation with similar units in southern Turkey. In: Göncüoğlu MC, Derman AS, editors. Early Paleozoic Evolution in NW Gondwana. TAPG Special Publication 3, pp. 50–60 (in Turkish).

Krynine PD (1949). The origin of red beds. Trans NY Acad Sci 11: 60–68.

Larsonneur C (1975). Tidal deposits, Mont Saint-Michel Bay, France. In: Ginsburg RN, editor. Tidal Deposits: A Casebook of Recent Examples and Fossil Counterparts. New York: Springer, pp. 21–30.

Mamet B, Preat A (2006). Iron-bacterial mediation in Phanerozoic red limestones: state of the art. Sediment Geol 185: 147–157.

Mamet B, Preat A, De Ridder C (1997). Bacterial origin of the red pigmentation in the Devonian Slivenec Limestone, Czech Republic. Facies 36: 173–188.

McBride EF (1974). Significance of color in red, green, purple, olive, brown, and gray beds of Difunta Group, northeastern Mexico. J Sediment Petrol 44: 760–773.

Miot J, Benzerara K, Morin G, Kappler A, Bernard S, Obst M, Ferard C, Skouri-Panet F, Guigner JM, Posth N, Galvez M, Brown GE Jr, Guyot F (2009). Iron biomineralization by anaerobic neutrophilic iron-oxidizing bacteria. Geochim Cosmochim Acta 73: 696–711.

Myrow PM (1990). A new graph for understanding colors of mudstones and shales. J Geol Educ 38: 16–20.

Özgül N (1983). Stratigraphy and tectonic evolution of the Central Taurides. In: Tekeli O, Göncüoğlu MC, editors. Proceedings of the International Symposium on the Geology of the Taurus Belt, Ankara, pp. 77–90.

Pettijohn FJ, Potter PE, Siever R (1987). Sand and Sandstone. New York: Springer.

Preat A, Mamet B, Bernard A, Gillan D (1999). Bacterial mediation red matrices diagenesis, Devonian, Montagne Noire (southern France). Sediment Geol 126: 223–242.

Preat A, Mamet B, De Ridder C, Boulvain F, Gillan D (2000). Iron bacterial and fungal mats, Bajocian stratotype (Mid-Jurassic, northern Normandy, France). Sediment Geol 137: 107–126.

Pye K (1983). Red beds. In: Goudie AS, Pye K, editors. Chemical Sediments and Geomorphology. London: Academic Press, pp. 227–263.

Robb GL (1949). Red bed coloration. J Sediment Petrol 19: 99–103.

Rogers JR, Bennett PC (2004). Mineral stimulation of subsurface microorganisms: release of limiting nutrients from silicates. Chem Geol 203: 91–108.

Santelli CM, Welch SA, Westrich HR, Banfield JF (2001). The effect of Fe-oxidizing bacteria on Fe-silicate mineral dissolution. Chem Geol 180: 99–115.

Schwertmann U (1993). Relation between iron oxides, soil color, and soil formation. In: Bigham JM, Ciolkosz EJ, editors. Soil Color. Madison, Wisconsin, USA: Soil Science Society of America, pp. 51–69.

Schwertmann U, Taylor RM (1989). Iron oxides. In: Dixon JB, Weed SB, editors. Minerals in Soil Environments. Madison, Wisconsin, USA: Soil Science Society of America, pp. 379–438.

Stumm W, Morgan JJ (1996). Aquatic Chemistry: Chemical Equilibria and Rates in Natural Waters. New York: John Wiley & Sons.

Tucker ME (1991). Sedimentary Petrology: An Introduction to the Origin of Sedimentary Rocks. Oxford: Blackwell.

Turner P (1979). Diagenetic origin of Cambrian marine red beds: Caerfai Bay shales, Dyfed Wales. Sediment Geol 24: 269–281.

Turner P (1980). Continental Red Beds. Amsterdam: Elsevier.

Van Houten FB (1968). Origin of red beds. Geol Soc Am Bull 79: 399–416.

Van Houten FB (1973). Origin of red beds: a review 1961–1972. Annu Rev Earth Planet Sci 1: 39–61.

Walker TR (1967). Formation of red beds in modern and ancient deserts. Geol Soc Am Bull 78: 353–368.

Walker TR, Larson EE, Hoblitt RP (1981). Nature and origin of hematite in the Moenkopi Formation (Triassic), Colorado plateau: a contribution to the origin of magnetism in red beds. J Geophys Res 86: 317–333.

Wehrmann A, Yılmaz I, Yalçın MN, Wilde V, Schindler E, Weddige K, Demirtaş GS, Özkan R, Nazik A, Nalcıoğlu G, Kozlu H, Karslıoğlu Ö, Jansen U, Ertuğ K (2010). Devonian shallow-water sequences from the North Gondwana coastal margin (Central and Eastern Taurides, Turkey): Sedimentology, facies and global events. Gondwana Res 17: 546–560.